JMEPEG (2009) 18:305–311
DOI: 10.1007/s11665-008-9272-y

1059-9495/$19.00

Effect of Microstructure on the Solid Particle Erosion Properties of Ni Plating

Feng Cai, Xiao Huang, Qi Yang, and Doug Nagy

(Submitted May 14, 2007; in revised form July 4, 2008)

The effect of microstructure on erosion resistance of nickel plating was investigated in this study. Two electrode nickel plating processes, one with conventional nickel sulfamate electrolyte and the other with carbon nanotubes (CNTs) dispersed in the electrolyte, at various pulse frequencies were used to generate surface depositions of different microstructures. The samples were subjected to microstructural evaluations and mechanical property testing for microhardness and elastic modulus. Subsequently, erosion tests were conducted to evaluate the material's erosion resistance under various plating conditions. It was found that both changes in pulse frequency and the addition of CNTs resulted in grain size refinement and surface morphology modification. Microhardness of the plating was observed to increase with the pulse frequency in the absence of CNTs. Erosion resistance increased with grain refinement initially due to the surface hardness increase but this effect subsided as the thickness of the deposition approached that of the plastic deformation layer caused by the erodent.

Keywords erosion resistance, grain size, nano grain structure, nickel electroplating, pulsed deposition

1. Introduction

Nickel electroplating plays an important role in providing steels with improved environmental protection. Nickel was first successfully plated onto a metal substrate in 1837; since then significant process development in nickel plating has been carried out to modify the microstructure and enhance the properties. It has been reported that by applying pulsed DC current during plating both coating surface morphology and hardness can be improved (Ref 1, 2) as the pulsed current increases nucleation rate and refines the grain structure (Ref 3, 4). For a certain plating condition, there exists a critical pulse frequency at which the nucleation rate reaches its peak value.

However, the hardness enhancement to the nickel plating achieved through process modification can be limited due to the intrinsic properties of pure nickel. To further improve the mechanical properties of nickel plating, alloying elements or particulates are incorporated into the nickel plating process. One of the notable examples is to incorporate carbon nanotubes (CNTs) or other micro- or nano-scaled particles into the plating process forming a composite surface deposition (Ref 5-8). In electrode plating process with CNTs two mechanisms can be involved: first, the randomly suspending CNTs in the electrolyte contact the substrate and are deposited by van der Waals force, and are further buried with the incoming ions; second, the suspending CNTs in the electrolyte attach to the ions in the electrolyte and move toward the substrate by Columbic force. It is believed that the combinations of both mechanisms contribute to the deposition process and impart changes to the nucleation and formation of new grain (Ref 2, 5).

Despite large number of research publications in the literature on nickel plating processes, the focus was mainly on the microstructure changes and hardness enhancement. Very limited research, however, has been carried out to examine the wear resistance, particularly the solid particle erosion resistance, of nickel plating with different microstructures. Solid particle erosion is defined as a progressive loss of original material from the surface due to the mechanical interaction between the surface and solid particles in relative motion (Ref 9). Erosion can change surface dimension, cause substantial material loss, and contribute to fatigue failure of components. The detrimental effect of erosion has been observed frequently in gas turbine engines and helicopter rotors operated in dessert or winter season when a deicing agent is used (Ref 10-12).

Solid particle erosion is generally divided into two types: ductile and brittle. In ductile erosion mode, the impacting solid particles in general cause localized plastic deformation to the material's surface. When the deformation eventually exceeds the strain to failure for the deformed materials, thin platelets will fracture and be removed by succeeding particles. To overcome ductile erosion, higher surface hardness is most desirable. Depending on the nature of the solid particle and the impingement angle (angle between direction of the incoming solid particle and the surface being eroded), cutting action of the eroding particles can also occur. For ductile erosion mode, the most severe damage occurs at 30° impingement angle (Ref 13-18). In brittle erosion mode, the eroding particles cause cracking and chipping of micro-sized pieces from material's surface as such material with higher fracture toughness is usually more resistant to erosion.

Feng Cai and **Xiao Huang**, Department of Mechanical & Aerospace Engineering, Carleton University, 1125 Colonel By Drive, Ottawa, ON, Canada K1S 5B6; **Qi Yang**, Institute for Aerospace Research, National Research Council Canada, 1200 Montréal Road, Ottawa, ON, Canada K1A 0R6; and **Doug Nagy**, Liburdi Turbine Services, Dundas, ON, Canada. Contact e-mail: fcai@connect.carleton.ca.

The current research was initiated to investigate the effect of various plating process parameters and the incorporation of CNTs on the microstructure and erosion resistance of nickel plating. Since the hardness value has direct influence on the erosion resistance of ductile materials, pulsed current and addition of CNTs in electrode plating were employed in this study to enhance the hardness of the nickel plating.

2. Experimental

2.1 Materials

The substrate is made of 1.5 mm thick mild steel sheet. The sheet metal was sheared to 76 mm in length and 25 mm in width. The sample surface was first polished with series of sand papers up to #600 grit size and then finished with 0.3 μm alumina slurry. Commercially pure nickel balls were used as the anode during nickel plating. The electrolyte contains 367 g/L nickel sulfamate ($Ni(NH_2SO_3)_2$), 12 g/L nickel chloride ($NiCl_2 \cdot 6H_2O$), and 36 g/L boric acid (H_3BO_3). The pH value of the electrolyte was adjusted to 1.5 at room temperature. The CNTs are single-walled nanotubes produced with electric-arc discharge technique (Ref 19). About 0.5 g CNTs, mixed with 0.08 g polyacrylic acid initially, were dispersed into 250 mL electrolyte. The electrolyte was further mixed under magnetic stirring at the rate of 600 rpm for 2 h prior to the deposition process. The method for dispersing CNTs in nickel sulfamate solution through acidic activation of the CNT surface and mechanical agitation are further reported by other researchers (Ref 20-22).

2.2 Equipment Setup

The plating apparatus consists of a power supply, an electrolyte bath, and the magnetic agitation unit. The power supply system is composed of a DC power supply, a function generator, and a solid state relay. The DC power supply provides direct current to the electrolyte bath. The required value of direct current can be obtained by adjusting the output voltage. Frequency variation is achieved by the function generator. In this experiment, the peak current density was maintained at 0.015 A cm^{-2} with the pulse frequencies ranging from 0, 5, 100 to 1000 Hz, respectively. The duty cycle was set to 50%. Table 1 summarizes the conditions in which the samples were plated.

Table 1 Experimental parameters and sample descriptions

Plating conditions	Peak current density, A/cm^2	Pulse frequency, Hz	Plating time, min
Ni plating series			
Ni-0	0.015	0	120
Ni-5		5	
Ni-100		100	
Ni-1000		1000	
Ni composite plating series with CNTs			
NiC-0	0.015	0	120
NiC-5		5	
NiC-100		100	
NiC-1000		1000	

Upon completion of the plating process, microstructure analysis was carried out. The surface morphology and microstructure were examined using a scanning electron microscope (SEM) (Philips XL30-SFEG). X-Ray diffraction (XRD) (Rigaku CN 2631 X-Ray diffractometer) was employed to investigate crystallographically preferred orientation and estimate the grain size of nickel plating. A Cu Kα x-ray source with a wavelength of 0.154 nm was used and the scan range, 2θ, was set from 30 to 100° with a rate of 1.8°/min.

The hardness and Young's modulus of the depositions were measured using a nano-hardness tester (CSM). A loading force of 20 mN and loading/unloading rate of 40 mN/min were selected and kept constant. The depths of indentation ranged from 0.2 to 0.50 μm. Twelve test points were taken for each sample and the average value is used in this study.

The erosion tests were conducted using an industrial type airbrasive unit (S.S. White model HME). In average three samples from each process condition were tested and the average value of the volume loss was used to represent the erosion rate. The erodent was angular aluminum oxide (Al_2O_3) particles with nominal particle size of 50 μm (AP106, S.S. White Technologies), and the carrying medium was compressed nitrogen at room temperature. The velocity of the erodent was controlled by the outlet pressure of the carrying gas and maintained at 30 ms^{-1} for this study. The feed rate of erodent was adjusted by controlling the voltages of the electrical vibrator to 80 V and the actual feed rate used was about 0.5 g/min. The mild steel samples were mounted on a holder that defines the particle attack/impingement angle and distance. In this experiment, the distance was set to 37.5 mm with an impingement angle of 30° since for ductile erosion mode, 30° impingement angle yields the highest erosion rate. The consumed mass of erodent was determined by the duration of the erosion test.

3. Results and Discussion

3.1 Surface Morphology

The conventional pure nickel electrodepositions exhibit surface morphologies which are dependant on the pulse frequency. As shown in Fig. 1, nickel plating obtained with pulsed current reveals much finer surface features, and this change in surface smoothness continues to increase with the pulse frequency in the range used in this study. The observed trend of increased surface smoothness with pulse frequency was also previously reported (Ref 4).

Figure 2 shows the surface morphologies of the nickel composite depositions with CNTs produced at various pulse frequencies. It illustrates the difference in surface morphology arising from pulsed current and the addition of CNTs. Naturally grown grain morphology, observed in Fig. 1(a), was less distinct with the addition of CNTs in the plating electrolyte. Instead, the surface, shown in Fig. 2(a), is composed of finer spherical grains. With the application of pulsed current, finer surface morphologies are observed in Fig. 2(b)-(d), similar to that found in Fig. 1(b)-(d). A distinguishable difference from the conventional nickel plating is the large clusters of CNTs observed on the surface indicating limited dispersion of CNTs in the electrolyte. It is also to be noted that the CNT cluster size varies from sample to sample as shown in Fig. 1.

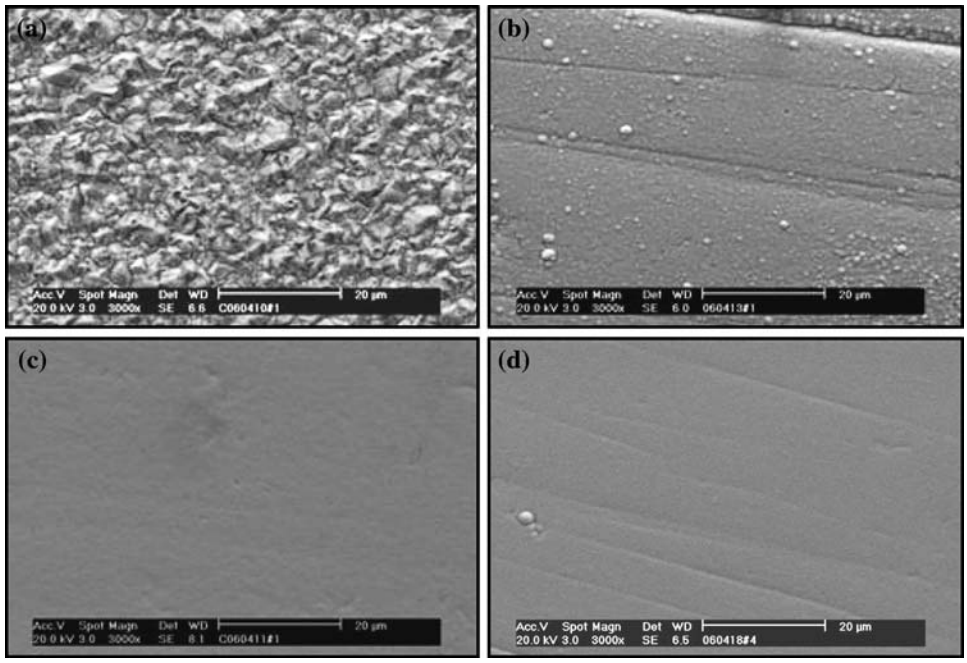

Fig. 1 SEM images of conventional nickel electroplating in the as-deposited condition. (a) Ni-0, (b) Ni-5, (c) Ni-100, and (d) Ni-1000

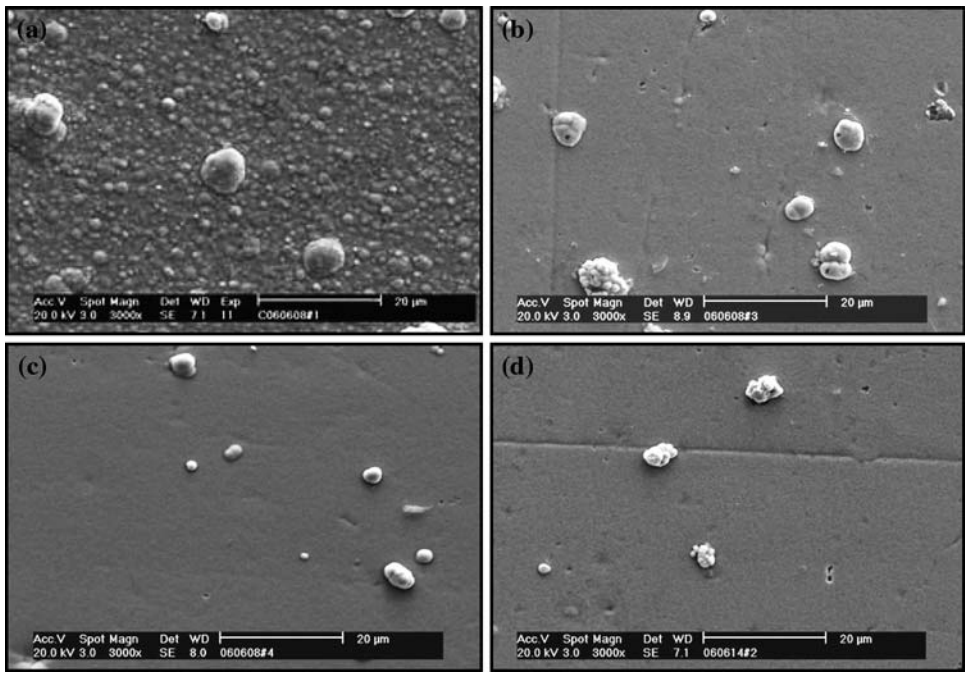

Fig. 2 SEM images of nickel electroplating with CNTs dispersed in the solution. (a) NiC-0, (b) NiC-5, (c) NiC-100, and (d) NiC-1000

The thicknesses of the plated samples were measured from the polished cross sections and the results are summarized in Fig. 3 and Table 2. As seen from Fig. 3 both pulse frequency and the incorporation of CNTs decrease the thicknesses (or deposition rate) of the plating within the same plating time; however, the extent of the thickness changes is different for the two types of plating. In the conventional nickel plating, deposition thickness is more sensitive to the pulse frequency and about 80% reduction in the plating thickness has resulted when changing from 0 (Ni-0) to 1000 Hz (Ni-1000) pulse frequency. The incorporation of CNTs to the electrolyte significantly reduced the plating thickness as demonstrated in Fig. 3. Additionally, for nickel plating with CNTs, the thickness decreases at a much slower rate with increasing pulse frequency.

3.2 Grain Size and Grain Orientation

Figure 4 and 5 illustrates the XRD patterns of the conventional nickel plating and nickel plating containing CNTs

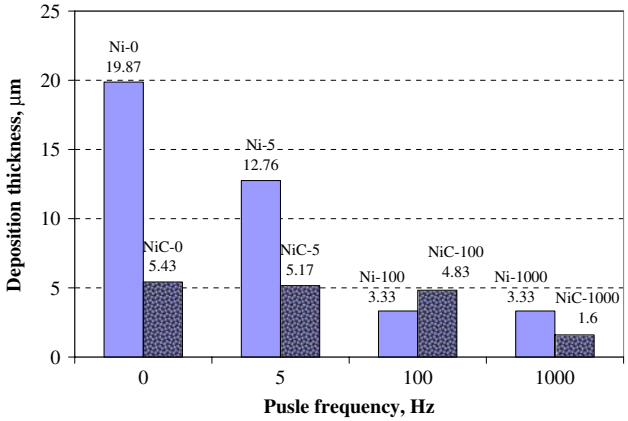

Fig. 3 Coating thickness changes with pulse frequency

Table 2 Grain size and residual micro strain in the plating

Plating conditions	Thickness, µm	Average grain size D, nm
Ni plating series		
Ni-0	19.9	51.3
Ni-5	12.8	34.7
Ni-100	3.3	18.5
Ni-1000	3.3	9.4
Ni composite plating series with CNTs		
NiC-0	5.4	10
NiC-5	5.2	48
NiC-100	4.8	19
NiC-1000	1.6	15.1

produced at various pulse frequencies. Distinct Ni (111) and Ni (200) peaks appear at $2\theta = 45°$ and 52°, respectively. From the XRD patterns, the full width at half maximum (FWHM) can be measured and used to calculate the average grain size of the nickel plating.

The broadening of X-ray diffraction peaks is affected by three factors: instrumentation, grain sizes, and residual micro strain. Their relationship can be described by (Ref 23):

$$\sqrt{B_o^2 - B_i^2} \cdot \cos(\theta) = \varepsilon \cdot \sin(\theta) + \frac{k\lambda}{D} \qquad \text{(Eq 1)}$$

where D is the average grain size (diameter) measured in a direction perpendicular to the surface of the specimen; k is a constant and a value of 0.9 was used in this study; B_o is the observed full width at half maximum (FWHM) and B_i is the instrumental broadening factor; θ is the Bragg angle; λ is the wavelength of the x-ray (for Cu Kα, $\lambda = 0.154$ nm); and ε is the residual strain. Applying experimentally measured FWHM at two Bragg angles, grain sizes were calculated with the results given in Table 2.

From the calculated values for grain sizes, it is apparent that the pulse frequency has played a controlling role in reducing the grain size of nickel plating. The grain size was reduced from 51 nm (Ni-0) to 9 nm (Ni-1000) when changing the pulse frequency from 0 to 1000 Hz. These results are in agreement with that reported in the literature (Ref 4, 24). The addition of CNTs reduced the grain size from 51 nm (Ni-0) to 10 nm (NiC-0) in the absence of pulsed current. There is no obvious trend observed in grain size changes with respect to the pulse frequency when CNTs are present in the electrolyte.

It is known that in isotropic polycrystalline nickel the intensity ratio between (111) and (200) peaks is 100:48 (Powder diffraction file PDF#04-0850, PDF-2 database sets 1-43, International Centre of Diffraction Data). Observing Fig. 4(a) it is clear that the grain growth of nickel plating was along a preferred [200] direction (perpendicular to (200) planes) during nickel plating for sample Ni-0. With the introduction of pulsed current, the amount of grains with the preferred [200] growth direction lessened gradually; however, even with the application of 1000 Hz pulse frequency for sample Ni-1000, this preferred orientation still remained by comparing the peak intensity ratio between (111) and (200) as shown in Fig. 4(d). The reason for such changes in crystal orientation is attributed to the continuous disruption of the grain growth along [200] direction when pulsed current is applied. The addition of CNTs in the electrolyte had less effect than pulsed current to disrupt grain growth in [200] direction as shown in Fig. 5(a) where lower Ni (200) peak was observed in sample NiC-0 than that in Fig. 4(a). It is also noted from the XRD spectra in Fig. 4 and 5 that additional peaks are observed near Ni (111) for sample Ni-1000 and NiC-1000. This additional peak was identified as diffraction of x-ray from mild steel substrate (BCC). With the increase of pulse frequency, the plating thickness reduced as illustrated in Fig. 3; therefore, the diffraction signal from the substrate intensified.

3.3 Hardness and Modulus of Elasticity

Microhardness values for samples obtained using different deposition parameters are presented in Fig. 6. For conventional nickel plating, the hardness seems to be more sensitive to the pulsing effect, and increased hardness values are observed with the increase of pulse frequency. This increase in hardness from 344 Hv (Ni-0) to 848 Hv (Ni-1000) is likely associated with grain size reduction, shown in Table 2, since fine-grained material has a greater total grain boundary area to impede dislocation motion.

The hardness is also significantly improved by the incorporation of CNTs when comparing Ni-0 to NiC-0; the hardness for plating containing CNTs shows an average hardness value of 760 Hv for NiC-0 while the hardness of Ni-0 is about 344 Hv. Referring to Table 2 sample NiC-0 has an average grain size of 10 nm while the grain size for Ni-0 sample is about 50 nm. In addition to finer grain size, sample NiC-0 also contains CNTs and they can impart additional dispersion hardening to the plating. The increase in hardness for plating with CNTs could therefore be resulted from the combination of grain size and dispersion hardening effects. In general the hardness is increased by the addition of CNTs, with the exception of sample NiC-1000. It is believed that this low hardness value for NiC-1000 is attributed to the low plating thickness (1.6 um), and the measured microhardness value was affected by the softer mild steel substrate. The significant influence from the limited plating thickness is further illustrated from the solid particle erosion results.

The Young's modulus, on the other hand, did not exhibit drastic changes with respect to pulse frequency. The most

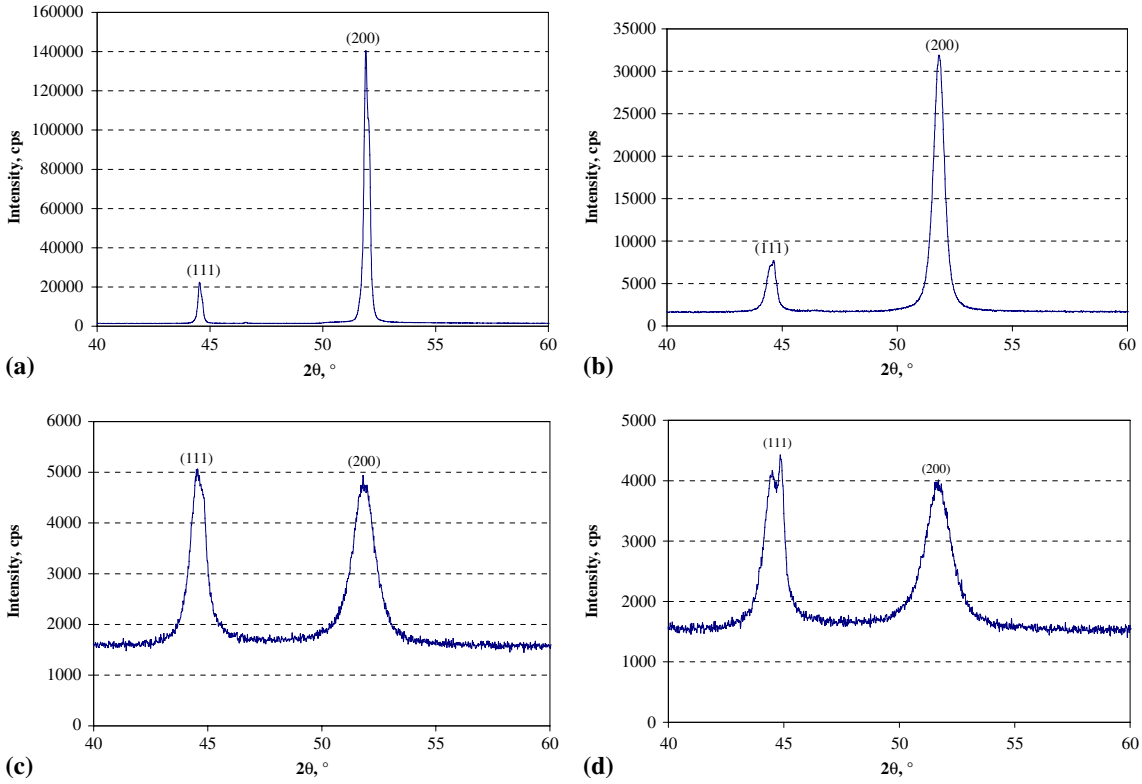

Fig. 4 XRD patterns of conventional nickel plating. (a) Ni-0, (b) Ni-5, (c) Ni-100, and (d) Ni-1000

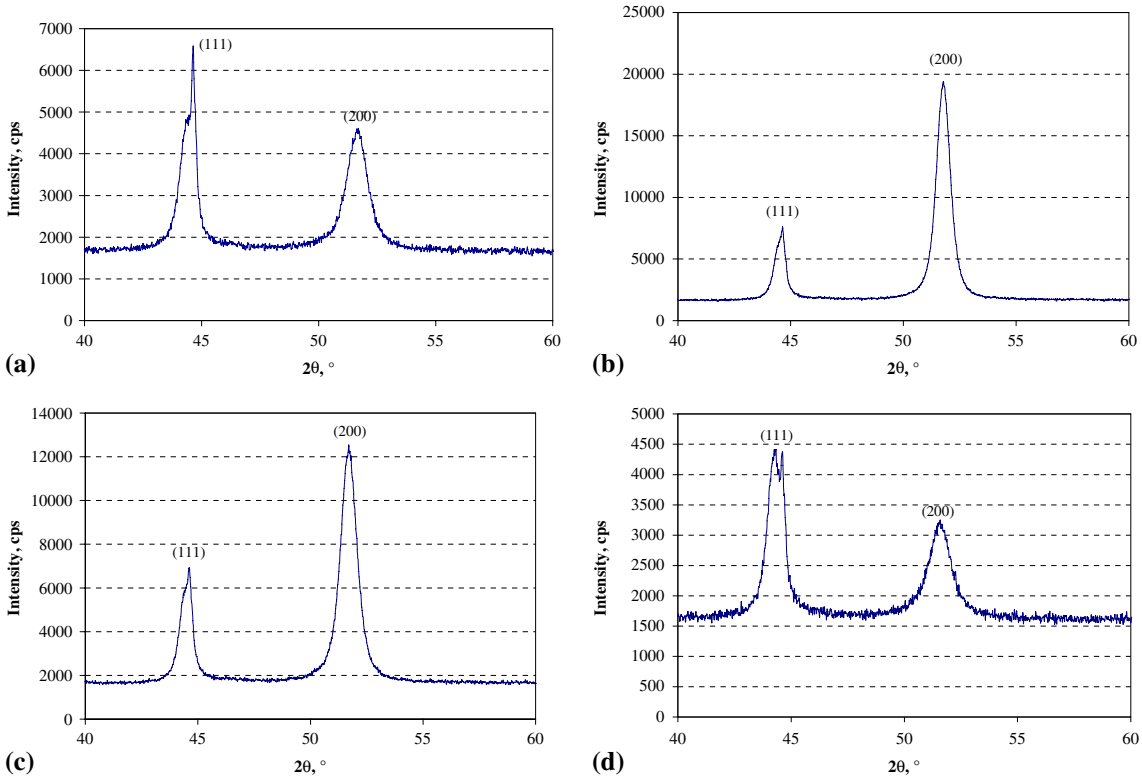

Fig. 5 XRD patterns of nickel plating with CNTs. (a) NiC-0, (b) NiC-5, (c) NiC-100, and (d) NiC-1000

noticeable observation from Fig. 6(b) is that the Young's modulus is higher for both samples Ni-0 and NiC-0. Pulsed current seems, in general, to have contributed to lower Young's modulus. The changes in Young's modulus for samples plated at various conditions are not as much as that in microhardness values.

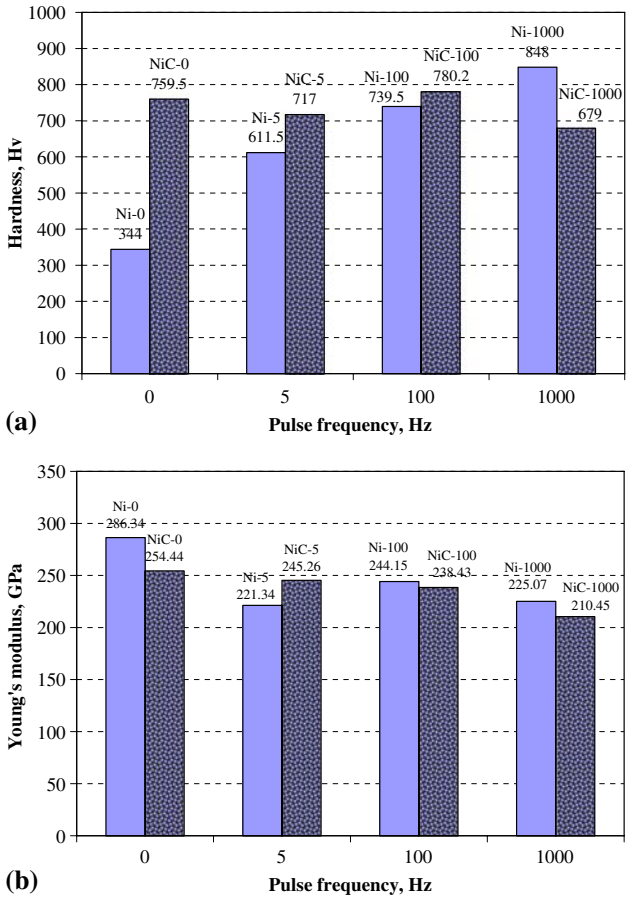

Fig. 6 (a) Microhardness and (b) Young's modulus for Ni-0, Ni-5, Ni-100, Ni-1000, NiC-0, NiC-5, NiC-100, and NiC-1000

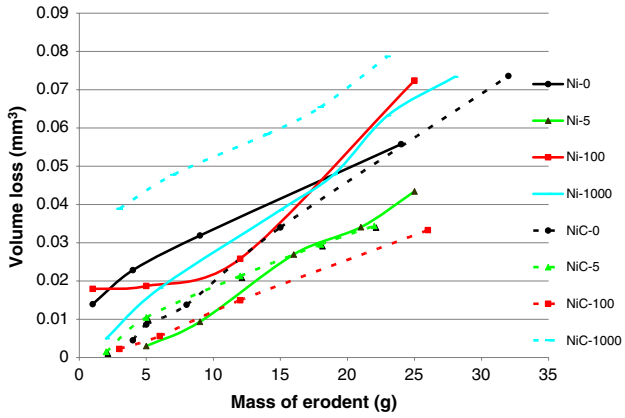

Fig. 7 Erosion rates as functions of erodent mass

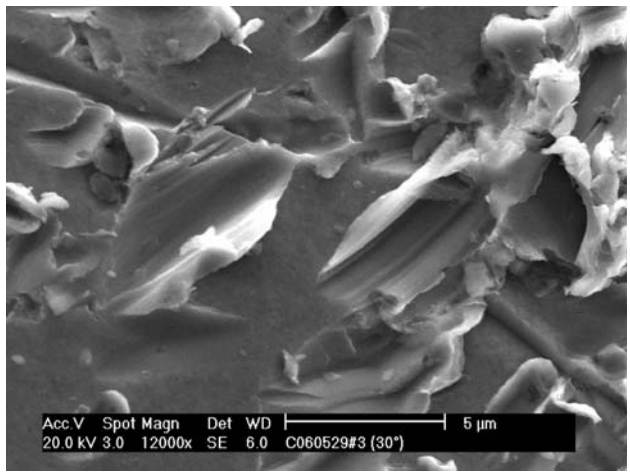

Fig. 8 Erosion morphologies of sample Ni-100 with attack angle at 30°

3.4 Erosion Resistance

The erosion rate of nickel plating was evaluated in terms of volume loss of the samples as a function of accumulated mass of erodent that attacks the sample at 30° impingement angle. The test results for both conventional nickel plating (solid lines) and nickel plating with CNTs (dashed lines) are shown in Fig. 7. For conventional nickel plated samples, Ni-5 exhibits the lowest erosion rate/volume loss while the other samples (Ni-0, Ni-100, and Ni-1000) have similar erosion volume loss. Examining the values of hardness given in Fig. 6(a), it is found that sample Ni-5 has substantially increased hardness than Ni-0, and the thickness value for Ni-5 (Table 2) is over four times that of Ni-100 and Ni-1000. The reduced erosion rate for Ni-5 is possibly due to the increased hardness (than Ni-0) and the higher plating thickness (than Ni-100 and Ni-1000). Since both Ni-100 and Ni-1000 have higher hardness value than Ni-5, it is speculated that the increased erosion rates for Ni-100 and Ni-1000 are as a result of reduced plating thickness. This has been reported in other studies (Ref 25).

To confirm that the limited plating thickness for Ni-100 and Ni-1000 has contributed to the increased erosion rate, an eroded surface was examined under SEM as shown in Fig. 8. From the surface morphology shown, it is clear that the depth of the impact from the solid particles is in the range of several µm. As the plating thicknesses for both Ni-100 and Ni-1000 were about 3.3 µm, it is likely that the solid particles have caused deformation to the substrate (mild steel). Since mild steel has lower hardness value (237 Hv) than nickel plating, the erosion resistance of thin plating can be compromised due to the influence from the substrate with lower resistance to plastic deformation.

Comparing the erosion performance between the two sets of samples with respect to the same pulse condition shown in Fig. 7, it is found that differences in erosion rate between samples Ni-0 and NiC-0 and samples Ni-5 and NiC-5 are minimal. Despite the higher hardness values for both samples NiC-0 and NiC-5, the erosion rate does not seem to change. It is not clear at present what role the CNTs played in the erosion process, particularly when the dispersion of CNTs is limited. At a pulse frequency of 100 Hz, a pronounced reduction in erosion rate for sample NiC-100, as compared to Ni-100, is observed (Fig. 7). In fact, sample NiC-100 had the lowest erosion rate among the samples tested in this study.

The increase in pulse frequency from 5 Hz to 100 Hz increased the hardness for both samples Ni-100 and NiC-100 and reduced the thickness of Ni-100 to 3.3 um and NiC-100 to 4.8 um. Both increased hardness and moderate plating thickness have contributed to the lower erosion rate for sample Ni-100. Further increasing the pulse current to 1000 Hz reduced the plating thickness for both Ni-1000 and NiC-1000. As seen in Fig. 7, sample NiC-1000 (with a plating thickness of 1.6 um) exhibits the highest erosion rate among all samples

tested, and the significant contribution of mild steel substrate to the erosion process is believed to be the origin for the high erosion rate observed. Due the variation in coating thickness values, it is not clear whether the Young's modulus has affected the erosion process of the nickel plating. In future study, the plating thickness is to be controlled so that the effects of microstructure and mechanical properties on erosion resistance of plating can be further studied.

4. Conclusions and Recommendations

In this study, electrode nickel plating was used to generate surface depositions with various microstructures. In addition to utilizing pulsed current during plating, CNTs were also incorporated into the nickel plating process to create a composite nickel plating. It was found that increasing pulse frequency during nickel plating had the effect of reducing the grain size of the plating and higher coating hardness. However, when CNTs were present in the electrolyte during nickel plating, this trend of decreasing grain size with pulse frequency was not observed. Instead, similar values of hardness and Young's modulus were observed despite the pulse frequency changes. While there was limited dispersion of CNTs in the nickel plating, CNTs were observed to have the effect of refining the grain size in the absence of pulsed current and increasing the hardness of the depositions. Both pulsed current and the addition of CNTs enhanced the plating surface smoothness. Erosion tests showed that two important factors contributed to the erosion rate. First the hardness of the plating played an important role in improving the erosion resistance, but it is also important to ensure that the thickness of the plating was sufficient to prevent substrate deformation by impinging solid particles during testing.

Future work should focus on controlling the plating process in such a way that constant thickness is produced under various plating conditions. The thickness should also be sufficient (>5 μm) so that the participation of substrate in plastic deformation during erosion test is eliminated. Secondly, the erosion test should be conducted at various impingement angles so that different erosion damage mechanisms can be studied.

Acknowledgments

The authors would like to thank Ontario Centers of Excellence (OCE) for providing financial support for this research. The supporting staff at the Department of Mechanical and Aerospace Engineering, Carleton University, particularly Mr. Fred Barrett and Steve Truttmann, have provided invaluable effort in the setup of the pulsed direct current power supply for this study.

References

1. A. Coehn, German Patent (75482), 1893
2. J.Cl. Puippe, Qualitative Approach to Pulse Plating, *Theory and Practice of Pulse Plating*, J.Cl. Puippe and F. Leaman, Eds., American Electroplaters & Surface Finishing Society, 1986
3. L. Shi, C. Sun, P. Gao, F. Zhou, and W. Liu, Mechanical Properties and Wear and Corrosion Resistance of Electrodeposited Ni-Co/SiC Nanocomposite Coating, *Appl. Surf. Sci.*, 2006, **252**, p 3591–3599
4. S.K. Ghosh, A.K. Grover, G.K. Dey, and M.K. Totlani, Nanocrystalline Ni-Cu Alloy Plating by Pulse Electrolysis, *Surf. Coat. Technol.*, 2000, **126**, p 48–63
5. A. Panda and E.J. Podlaha, Nanoparticles to Improve Mass Transport Inside Deep Recesses, *Electrochem. Solid-State Lett.*, 2003, **6**(11), p C149–C152
6. S. Arai, M. Endo, and N. Kaneko, Ni-deposited Multi-walled Carbon Nanotubes by Electrodeposition, *Carbon*, 2004, **42**, p 641–644
7. Y. Gan, D. Lee, X. Chen, and J.W. Kysar, Structure and Properties of Electrocodeposited Cu-Al_2O_3 Nanocomposite Thin Films, *J. Eng. Mater. Technol.*, 2005, **127**, p 451–456
8. P. Gyftou, M. Stroumbouli, E.A. Pavlatou, P. Asimidis, and N. Spyrellis, Tribological Study of Ni Matrix Composite Coatings Containing Nano and Micro SiC Particles, *Electrochim. Acta*, 2005, **50**, p 4544–4550
9. B.A. Lindsley and A.R. Marder, Solid Particle Erosion of an Fe-Fe3C Metal Matrix Composite, *Metall. Mater. Trans. A*, 1998, **29A**(3A), p 1071–1079
10. J.T. DeMasi-Marcin and D.K. Gupta, Protective Coatings in the Gas Turbine Engine, *Surf. Coat. Technol.*, 1994, **68/69**, p 1–9
11. V.R. Parameswaran, J.-P. Immarigeon, and D. Nagy, Titanium Nitride Coating for Aero Engine Compressor Gas Path Components, *Surf. Coat. Technol.*, 1992, **52**, p 251–260
12. V.R. Parameswaran, J.-P. Immarigeon, D. Chow, and D. Morphy, Erosion Coatings for Compressor Applications, *Advances in High Temperature Structure Materials and Protective Coatings*, A.K. Koul, V.R. Parameswaran, J.-P. Immarigeon, and W. Wallace, Eds., National Research Council of Canada, Ottawa, Canada, 1994
13. A.V. Levy, *Solid Particle Erosion and Erosion-Corrosion of Materials*. ASM International, 1995
14. C.M. Preece and N.H. Macmillan, Erosion, *Ann. Rev. Mater. Sci.*, 1977, **7**, p 95–121
15. W.F. Adler, Assessment of the State of Knowledge Pertaining to Solid Particle Erosion, Report No. CR 79-680, 30 June 1979, US Army Research Office Control DAA G29-77-C-0039
16. G.P. Tilly, Erosion Caused by Impact of Solid Particles in Wear, *Treaties on Material Science and Technology*, D. Scott, Ed., Vol. 13, Academic Press, 1979
17. S.M. Wiederhom and B.H. Hockey, Effect of Material Parameters on the Erosion Resistance of Brittle Materials, *J. Mater. Sci.*, 1983, **18**, p 766–789
18. D. Aquaro and E. Fontani, Erosion of Ductile and Brittle Materials, *Meccanica*, 2001, **36**, p 651–661. Kluwer Academic Publishers, Netherlands
19. Y. Pei, "Morphology and Mechanical Properties of Polycarbonate/Carbon Nanotube Composites," Thesis of Master of Applied Science, Carleton Univeristy, 2003, Ottawa, Canada
20. G.R. Shen, Y.-T. Cheng, and L.-N. Tsai, Synthesis and Characterization of Ni-P-CNT's Nanocomposite Film for MEMS Applications, *IEEE Trans. Nanotechnol.*, 2005, **4**(5), p 539–547
21. S. Arai and M. Endo, Carbon Nanofiber-Copper Composite Powder Prepared by Electrodeposition, *Electrochem. Commun.*, 2003, **5**, p 797–799
22. L. Wang, Y. Gao, Q. Xue, H. Liu, and T. Xua, Effects of Nano-diamond Particles on the Structure and Tribological Property of Ni-matrix Nanocomposite Coatings, *Mater. Sci. Eng. A*, 2005, **390**, p 313–318
23. C. Suryanarayana and M.G. Norton, *X-Ray Diffraction: A Practical Approach*, Plenum Press, New York and London, 1998
24. A.M. El-Sherik, U. Erb, and J. Page, Microstructural Evolution in Pulse Plated Nickel Electrodeposits, *Surf. Coat. Technol.*, 1996, **88**, p 70–78
25. K.L. Rutherford and I.M. Hutchings, Development of Erosion Durability Technique for Thin Coatings, *Surf. Coat. Technol.*, 1996, **86-87**, p 542–548